Spring 1-1-2020

Influence of Hydrogen Peroxide And Depletants on the Clustering of Active Janus Particles

Mohammed Kalil
Cleveland State University

INFLUENCE OF HYDROGEN PEROXIDE AND DEPLETANTS ON THE CLUSTERING OF ACTIVE JANUS PARTICLES

MOHAMMED KALIL

Bachelor of Science in Chemical Engineering

Cleveland State University

December 2019

Submitted in Partial Fulfillment of Requirements for the Degree

MASTER OF SCIENCE IN CHEMICAL ENGINEERING

At the

CLEVELAND STATE UNIVERSITY

May 2020

We hereby approve this thesis for

MOHAMMED KALIL

Candidate for the Master of Science in Chemical Engineering degree

for the Department of Chemical and Biomedical Engineering and

CLEVELAND STATE UNIVERSITY'S

College of Graduate Studies by

Thesis committee chairperson, Dr. Christopher Wirth

Department of Chemical and Biomedical Engineering

Department & Date

Thesis committee member, Dr. Nolan Holland

Department of Chemical and Biomedical Engineering

Department & Date

Thesis committee member, Dr. Shawn Ryan

Department of Mathematics

Department & Date

Student's Date of Defense: May 12, 2020

INFLUENCE OF HYDROGEN PEROXIDE AND DEPLETANTS ON THE CLUSTERING OF ACTIVE JANUS PARTICLES

MOHAMMED KALIL

ABSTRACT

Active Janus particles experience autonomous motion at scales where Brownian stochastic fluctuations typically dominate trajectories. This autonomous motion further drives a broad range of collective behavior in simple and complex environments. Such behavior of synthetic particles has been shown to closely mimic that of motile biological systems. Furthermore, active Janus particles have potential to drive innovation in existing applications, including transport in microscale environments. Herein, I will describe a series of experiments that delve into the ensemble behavior of active platinum-coated Janus particles, specifically, the influence of hydrogen peroxide and depletion forces on their clustering dynamics. These experiments are part of an effort to understand the influence of propulsion speed on collective behavior. I found the extent of clustering increased as hydrogen peroxide concentrations increased in the absence of depletion interactions. Depletion interactions, introduced by the addition of PEG, had a duel effect. At low volume fractions, the addition of PEG increased the probability of observing clusters by enhancing particle-to-particle attraction and cluster longevity. Yet, at high volume fractions where depletion interactions are previously known to quench swimming speeds, the extent of clustering was reduced as result of a diminished collision probability. These observations and conclusions reveal the nuanced affects $\sim kT$ scale interactions have on the collective behavior of propelling Janus particles.

TABLE OF CONTENTS

APPENDICES

LIST OF FIGURES

Figure Page

CHAPTER I

INTRODUCTION

Active particles are able to consume energy from their environment and convert it into a mechanical force, generating autonomous movement [1]. Autonomous motion is most often observed in animals, which experience a wide range of collective behavior such as swarming and flocking (ex. birds and fish) [2]. One example of autonomous motion is that of motility of microorganisms at the micro- and nano-scales, where motion is often randomized by Brownian fluctuations. Microorganisms such as bacteria exhibit motility in their search for nutrients relying on sensing mechanisms such as chemotaxis to navigate and move around their environment [2-3]. Recent progress in fabrication methods of materials has given us the ability to design micro swimmers to isolate and mimic self-propulsion as seen in biological systems [4-9]. Synthetic active particles offer an analogous model to study motile microorganisms and relevant collective behavior.

In both biological and synthetic active systems, active particles will interact with boundaries of their environment and each other leading to various collective behavior. For example, the bacteria *Capnocytophaga gingivalis*, found in the human biome, is observed to swarm near boundaries in specific structures that allow them to transport cargo without

growth or use of its flagella [10]. Similarly, synthetic swimmers have been shown to be steered and directed by nearby boundaries [11-12]. However, collective behavior is not limited to boundaries, as active particles have been observed to form clusters by colliding and trapping other particles [13-15]. Recent studies and demonstrations of active colloidal systems show potential of utility in the fields of waste removal and environmental remediation, lab-on-a-chip transport, and drug delivery [4, 15-20].

All synthetic swimmers require a source of energy (fuel) regardless of the method of self-propulsion implemented, whether it is hydrogen peroxide catalyzed by a platinum coated cap [4-9], or light absorbed by graphite caps to heat up and thereby demix near critical solutions [13, 21]. In both cases, the essential mechanism is to generate solute gradients around a given particle, thereby inducing diffusion of the particle up or down the solute gradient. This transport mechanism is called self-diffusiophoresis [21-22]. Thus, altering the concentration of the fuel, or illumination in the case of near critical solutions, can change the propulsion speed experienced by particles. This becomes especially important in devising self-propulsion systems, as previous work has shown that collective behavior, such as clustering, is hydrodynamic in nature and is a function of nominal speeds of the particles [13]. Herein, I set out to conduct experiments to demonstrate how the rate of clustering of platinum-coated Janus particles is affected by swimming speed by varying the hydrogen peroxide concentration and the addition of a nanoparticle to induce changes in ~kT scale interactions. The main intellectual contributions derived were the following:

- Clustering was observed to increase with the concentration of hydrogen peroxide.
- Polyethylene glycol (PEG) is a polymer commonly used as a depletant, previously observed to quench the swimming speeds of active Janus particles [23]. To

demonstrate the correlation between swimming speeds and clustering, I introduced PEG (6k molecular weight) along with hydrogen peroxide as in the first set of my experiments, with the expectations of reduced clustering. The results did show reduced clustering in PEG volume fraction ranges previously reported to quench swimming speeds. However, when tested with volume fractions below, clustering appeared to be enhanced.

CHAPTER II

THEORY/LITERATURE REVIEW

2.1 Active particles

With synthetic micro swimmers comes a great deal of variability. Different methods of propulsion can be employed based on the application's need, along with various shapes and sizes of particles. So far, published work on active particles has demonstrated multiple ways of achieving self-propulsion that can all be classified into three main different classes [22].

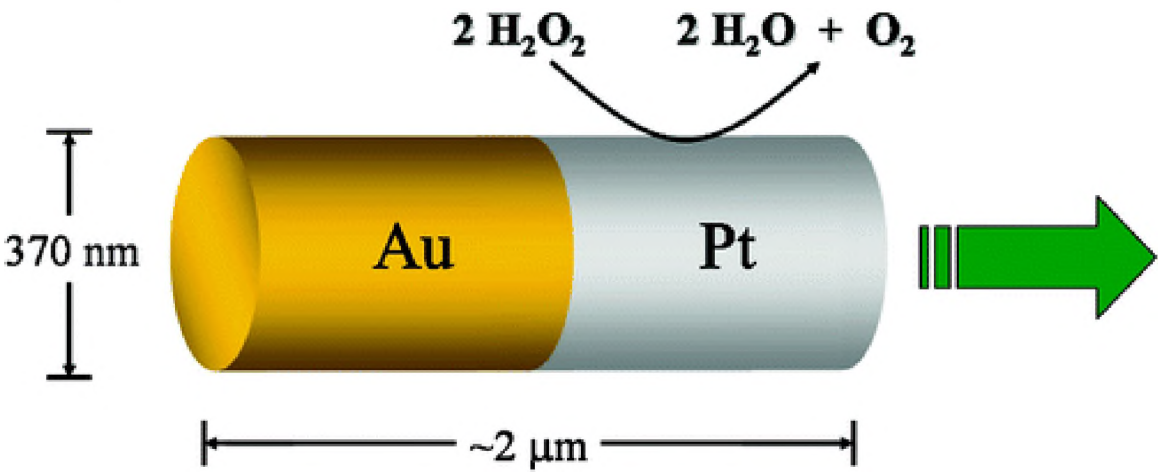

Figure 1: An example of a bimetallic active nanorod. This was one of the earliest types of synthetic swimmers devised by Paxton et al (2004). The platinum end oxidizes hydrogen peroxide, producing hydronium cations and electrons. These products defuse to the gold end where they are reduced back to hydrogen peroxide, creating a slip velocity on the swimmer rod. Reprinted with permission from [1] Paxton, W.; Kistler, K.; Olmeda, C.; Sen, A.; St. Angelo, S.; Cao, Y.; Mallouk, T.; Lammert, P.; Crespi, V. Catalytic Nanomotors: Autonomous Movement Of Striped Nanorods. Journal of the American Chemical Society 2004, 126 (41), 13424-13431. Copyright (2004) American Chemical Society.

The first class achieves motility through self-electrophoresis in bi-segmented metallic rods (**Figure 1**) with each rod acting as a redox pair, creating self-generated electric fields [1, 24]. The second class is through asymmetric bubble production through a fuel decomposition by a catalyst, usually platinum catalyzing high enough concentrations of hydrogen peroxide to oxygen gas [25-28]. **Figure 2** shows an example of how a platinum/polystyrene dimer can swim in different directions based on the nucleation location of the periodic bubble formation

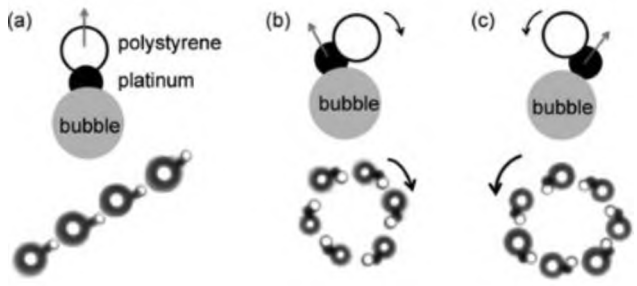

Figure 2: Propulsion by bubble production in polystyrene and platinum dimers. These active particles move by the periodic formation and breakdown of bubbles formed on the platinum end, causing it to move forward, or spin around. Reprinted with permission from [25] Wang, S.; Wu, N. Selecting The Swimming Mechanisms Of Colloidal Particles: Bubble Propulsion Versus Self-Diffusiophoresis. Langmuir 2014, 30 (12), 3477-3486. Copyright (2014) American Chemical Society.

The third class is based on the self-generation of solute gradients on the surface of swimmers (self-diffusiophoresis) [7, 15, 21-22, 29]. For example, graphite capped Janus particles are used to demix a near critical mixture of water and 2,6-lutidine by illuminating the particles with a beam of 532 nm, the wavelength which the graphite absorbs, generating heat that demixes the solution, producing solute gradients around swimmers [13]. In this study, clustering was observed as a result of self-propulsion. Furthermore, data showed evidence that clustering was hydrodynamic in nature, directly proportional to the swimming speed of the particles. Another example of the third class of micro swimmers is Janus spheres coated with a catalyst on one side such as platinum, creating solute gradients by consuming a fuel such as hydrogen peroxide and creating new products (oxygen and water) [7, 29]. This method of propulsion is what my work is mostly concerned with. It is very similar to the second class of swimmers, except it is carried out

in lower hydrogen peroxide concentrations, where bubble production is not sufficient to move the particles.

2.1.1 Self-diffusiophoresis

Previous studies have demonstrated that self-diffusiophoresis is the type of motion experienced by active platinum-coated Janus particles in hydrogen peroxide. This type of motion occurs as a result of concentration gradients surrounding the swimmer [22].

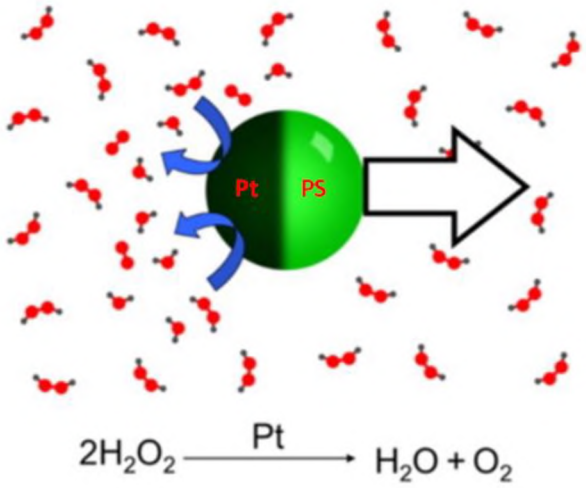

Figure 3: An illustration of self-diffusiophoresis in active Janus particles. The platinum end decomposes the hydrogen peroxide into oxygen and water, causing concentration gradients of the products around the particles, driving a slip velocity that causes the particles to swim forward. Reprinted with permission from [4] Ebbens, S. Active Colloids: Progress And Challenges Towards Realising Autonomous Applications. Current Opinion in Colloid & Interface Science 2016, 21, 14-23.. Copyright (2016) Elsevier.

As observed in **Figure 3**, a swimmer particle decomposes hydrogen peroxide according to the equation shown in the same figure, leaving behind water and oxygen. This causes gradients of the products around the particle accumulating on the platinum end. As the products diffuse away, a slip flow is felt by the particle causing it to move forward.

2.1.1.1 Neutral vs ionic self-diffusiophoresis

There are two types of self-diffusiophoresis, neutral and ionic. Neutral is when the solutes are uncharged. Ionic self-diffusiophoresis is when ionic products are produced by the reaction. A study into the decomposition of hydrogen peroxide by platinum suggests that the reaction is electrochemical by nature, and it has an alternate pathway, producing charged intermediates as shown in **Figure 4** [30].

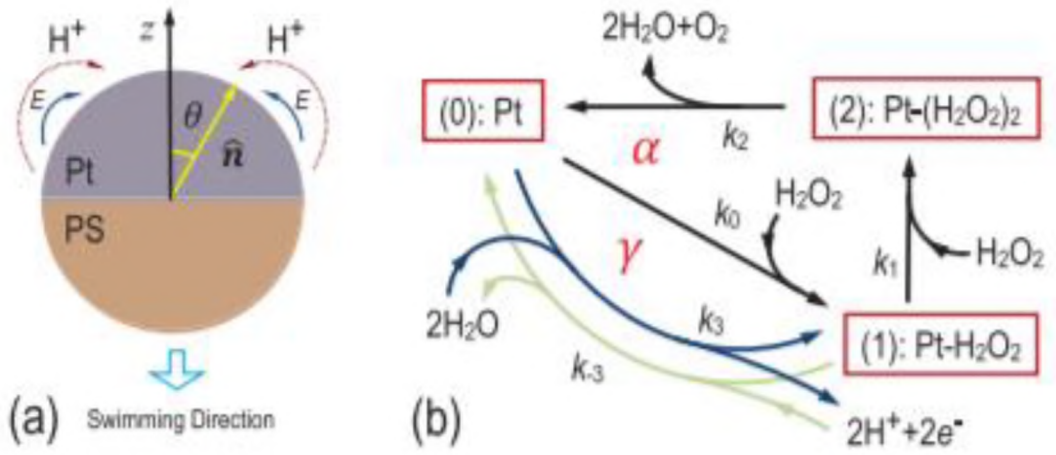

Figure 4: a) A schematic of a Pt/PS Janus particle showing the direction of flow of the ions and the electric field. b) The reaction scheme showing both pathways possible for the decomposition of hydrogen peroxide. Loop α is the main nonequilibrium cycle, while loop γ is linked to the production of charged intermediates [30]. Reprinted with permission from [30] Ebbens, S.; Gregory, D.; Dunderdale, G.; Howse, J.; Ibrahim, Y.; Liverpool, T.; Golestanian, R. Electrokinetic Effects In Catalytic Platinum-Insulator Janus Swimmers. EPL (Europhysics Letters) 2014, 106 (5), 58003.. Copyright (2014) EPLA.

The study concluded that motion of Pt/PS particles is due to a combination of both neutral and ionic self-diffusiophoresis. Furthermore, their conclusion believed that the

ionic effects were strong enough that self-electrophoretic effects also played a major part in their motion, which is supported by other work [11, 22, 24, 30-32].

2.1.2 Self-Electrophoresis

As previously mentioned, studies have demonstrated ionic effects' role in the propulsion of catalytic Janus particles. As shown in **Figure 5**, electric fields arise due to the separation of charge resulting from changes in the transport rate of the charged pair [22, 31]. This electric field acts on the diffuse layer of the Janus particles and drives a motion forward.

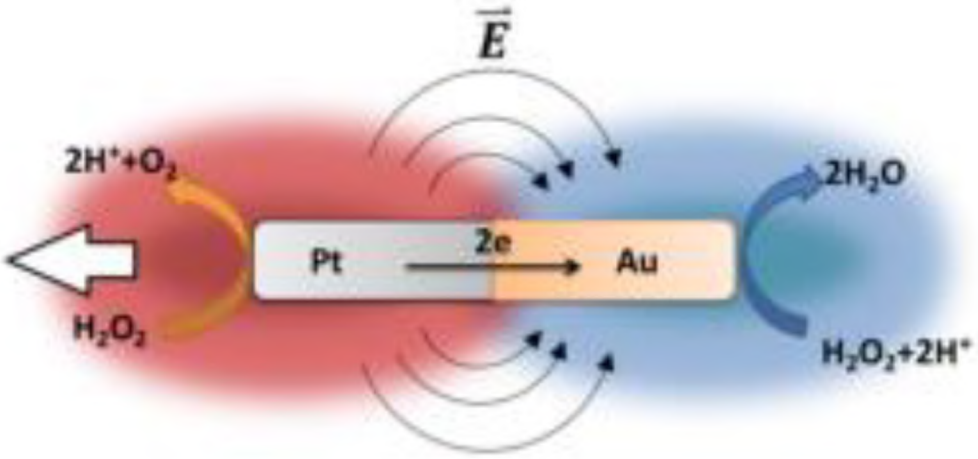

Figure 5: An illustration of self-electrophoresis in bimetallic rods. Platinum oxidizes the fuel, hydrogen peroxide, into protons in solutions (hydronium cations), and electrons that conduct to the gold end of the rod. There, the electrons along with the hydronium ions in solution diffusing across the rod to the gold end are reduced back to hydrogen peroxide. The resultant ion gradient creates an electric field force acting on the diffuse layer of the Janus particles, driving a slip flow. Reprinted with permission from [31] Chiang, T.; Velegol, D. Localized Electroosmosis (LEO) Induced By Spherical Colloidal Motors. Langmuir 2014, 30 (10), 2600-2607.. Copyright (2014) American Chemical Society.

The extent of contribution to either neutral or ionic self-diffusiophoresis and self-electrophoresis remains a hotly debated topic within the active particle community. While most studies agree that an interplay of all three types of motion is in effect [11, 22, 30], one study has argued against both neutral and ionic self-diffusiophoresis and suggested instead that motion is self-electrophoretic, much like the case of the oxidizing bimetallic rods, after they reversed the direction of propulsion of Janus particles by adding salts [32]

2.2 Complex environments and collective behavior

Due to the autonomous motion active particles enjoy, they display unique behavior non-active particles cannot. For the most part, in simple environments such as the bulk, active particles enjoy enhanced diffusion [15]. As particles shift from Brownian motion to a deterministic walk, they are much more likely to run into other particles and boundaries while also experiencing non-conservative surface interactions [15, 33-34]. These interactions lead to the unique behavior mentioned above, some of which will be mentioned in the next subsections:

2.2.1 Particle to particle interactions: Clustering and "living crystals"

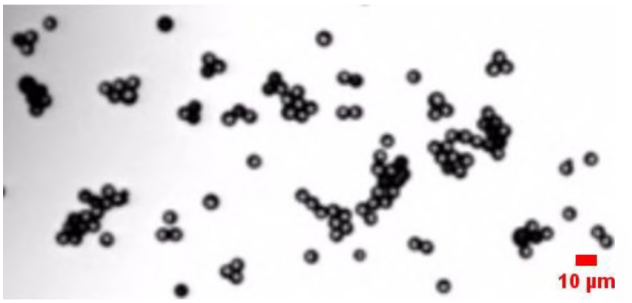

Figure 6: An image of a dilute suspension of 5 µm platinum coated particles in 3% v/v H_2O_2 showing cluster formations. Clusters can be seen of multiple different sizes.

Unlike passive particles, a dilute suspension of active swimmers can form clusters (**Figure 6**) even in the presence of repulsive forces [35]. A simple explanation for this phenomenon is considering the collision dynamics of particles. When two particles collide head on, they block each other, forming a temporary two particle cluster. Particles will re-orient themselves away from each other and eventually swim apart on the time scale of the rotational diffusion (**Figure 7**). However, depending on the particle speed and density, the mean collision time could be fast enough that another particle joins the cluster before the two first particles could break apart, building larger clusters that could rearrange and exchange particles, gaining the name "living crystals" [36]. DLVO and near-field hydrodynamics also can play a crucial role in determining the rate of clustering, while some studies have also shown diffusiophoretic aggregation mechanism which is caused by the interaction of the concentration profiles around the particles [37-41].

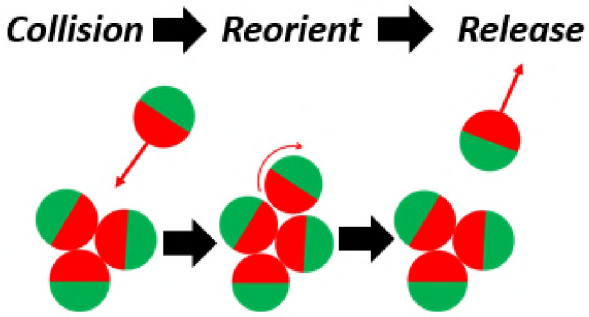

Figure 7: An illustration showing the collision dynamics of active Janus particles. Particles collide, forming larger clusters that eventually merge and exchange particles with other clusters or the bulk.

2.2.2 Particle near a boundary

Particles approaching a boundary behave differently than particles in the bulk. While sometimes, far-field hydrodynamic effects are capable of course correcting, the most

prominent effects are near-field and steric interactions leading to a broad range of behavior such as trapping, wall scattering and hovering [15, 42]. As a particle approaches a wall or a boundary, the hydrodynamic interactions will align the particle to swim along the boundary (rheotaxis). However, there is an asymmetry between particles approaching and leaving the wall [12]. When approaching, a particle's path will become stuck to the wall unless its orientation is changed, and the particle swims away from the wall (wall scattering). When a particle leaves the wall, it simply swims away. This asymmetry results in a tendency for active particles to accumulate near confining boundaries [15, 43-45].

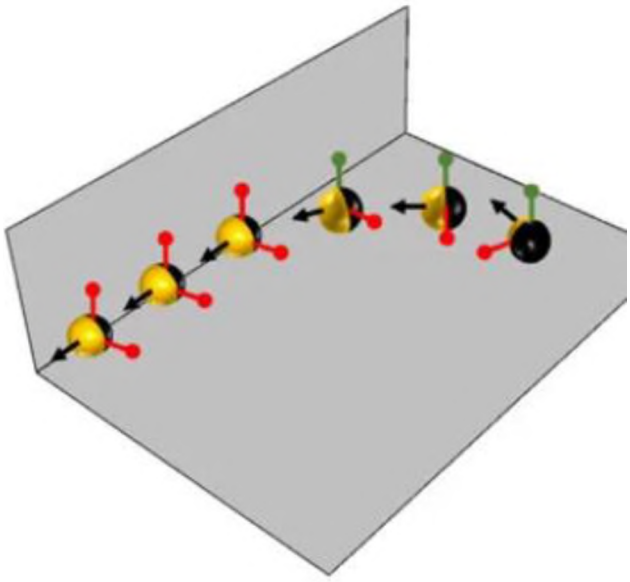

Figure 8: Steric interactions are known to quench the rotational diffusion. Limiting the degrees of freedom particles have to move enhances the deterministic diffusion of particles along the wall. In this figure, a red axis represents a limited axis of rotation, while green is unlimited. Reprinted with permission from [11] Das, S.; Garg, A.; Campbell, A.; Howse, J.; Sen, A.; Velegol, D.; Golestanian, R.; Ebbens, S. Boundaries Can Steer Active Janus Spheres. Nature Communications 2015, 6 (1). Copyright (2015) Springer Nature.

A particularly interesting behavior that arises from active particles near boundaries is the quenching of their rotational diffusion (**Figure 8**). Steric interactions limit the degrees of freedom a particle has to move, enhancing their translation diffusion. A study has devised such geometric restriction as a method for steering active particles without an outside global steering method [11].

2.2.3 Depletion interactions

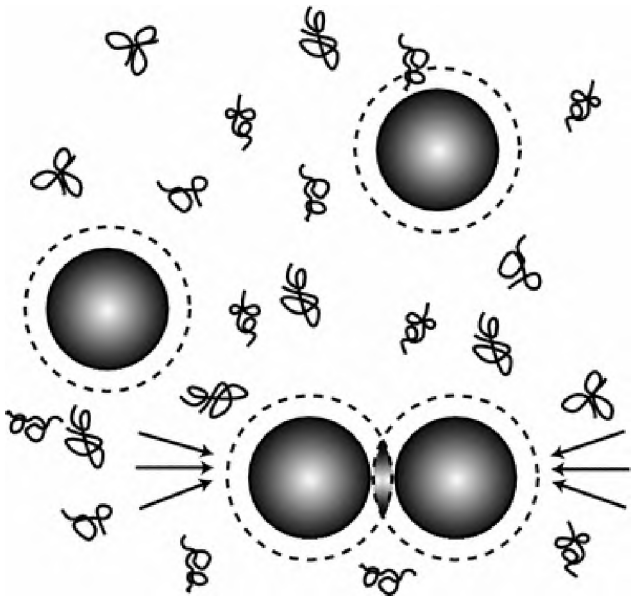

Figure 9: An illustration of depletion interaction which is an attractive force felt by two surfaces/particles. Depletants, usually smaller solutes surrounding larger colloidal particles increase the osmotic pressure between two surfaces when they are close enough that depletants are excluded from the space between the particles as shown in the pair of particles at the bottom of the illustration. Reprinted with permission from [46] Tuinier, R. Introduction To Depletion Interaction And Colloidal Phase Behaviour. Soft Matter at Aqueous Interfaces 2015, 71-106. . Copyright (2016) Springer Nature.

Depletion interactions can be added to active systems to introduce an attraction force felt between nearby surfaces. Depletants, usually a small polymer diluted in solution,

introduces an attractive force by increasing the osmotic pressure felt between two particles, or a particle and a surface. As particles get closer and consume the space between them, depletants are excluded from that volume between the particles, increasing the osmotic pressure [47-49]. **Figure 9** shows a visual demonstration of the depletion interaction between colloidal particles. At sufficient concentrations, depletants have been demonstrated to quench propulsion speeds without reducing the rate of activity in the system [23]. This will keep the same concentration of hydrogen peroxide in each experiment, the same rate of hydrogen peroxide breakdown, except with reduced speed, allowing us to isolate the effects of swimming speeds.

CHAPTER III

EXPERIMENTAL PROCEDURE AND INSTRUMENTATION

3.1 Fabrication of Janus particles

3.1.1 Monolayer Formation

The first step in preparing anisotropically platinum-coated polystyrene micro-particles is packing the spheres into monolayers on 20x20mm diced Silicon Wafer (Ted Pella, INC) (**Figure 10**). Spin coating is a well-documented monolayer formation technique and it is used here to prepare the particles for platinum deposition [50]. Particle size, humidity, temperature, particle concentration, number of steps, speed of each step and the total volume of solution deposited on each silicon wafer were all factors in determining the quality of the monolayer coverage.

The setup of the experiment demands more attention to be paid towards decreasing the number of defects and multi-layer sections, rather than increasing the percentage of the wafer covered. Doing so ensures ensemble behavior is not affected by the presence of non-active particles. However, ensuring high coverage percentages produces significantly more coated particles per each deposition, thus increasing efficiency. For that reason, a

good balance between increasing coverage, and limiting defects and multilayers is required.

First, particles were washed, and solvent exchanged to ethanol. The solution concentration was highly dependent on the particle size used. For this experiment, 5 μm diameter PS particle were chosen. Due to the lack of reported literature forming monolayers with that specific particle diameter, a trial and error method was implemented. Particle concentration testing started at 20% w/v, while systematically decreasing the concentration by 1%.

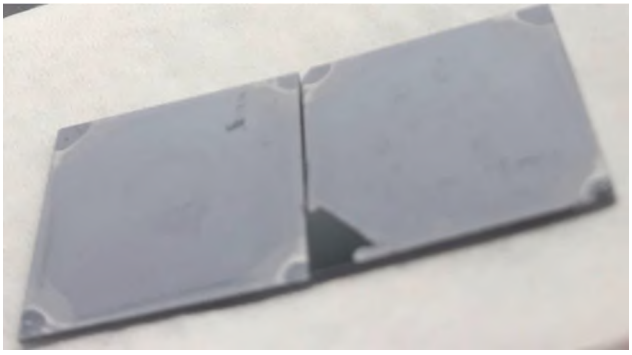

Figure 10: 20x20 mm wafers covered with monolayers of PS particles: The wafers above are from an experiment analyzing monolayer formation of a 14% w/v solution.

Resultant monolayers were analyzed under an SEM microscope (CSU Physics Department) for the ideal concentration. The ideal concentration reduced the disorder in the packing of the particles when viewed under the SEM microscope (**Figure 11**). At a temperature of 72° F and humidity of 48%, it was found that approximately 14% yielded the best results. Each concentration was tested depositing volumes between 15-25 μL, with 17 μL giving the best results. A two-step spin-coating method uses the first step to spread the particles around the wafer using low speeds, while the second step orders the particles into a monolayer using a high-speed step [50]. Based on previous work forming

monolayers with polystyrene particles within our lab, it was advised to use a first step of 300 RPMs for 15 seconds and a second step of 5000 RPMs for 40 seconds.

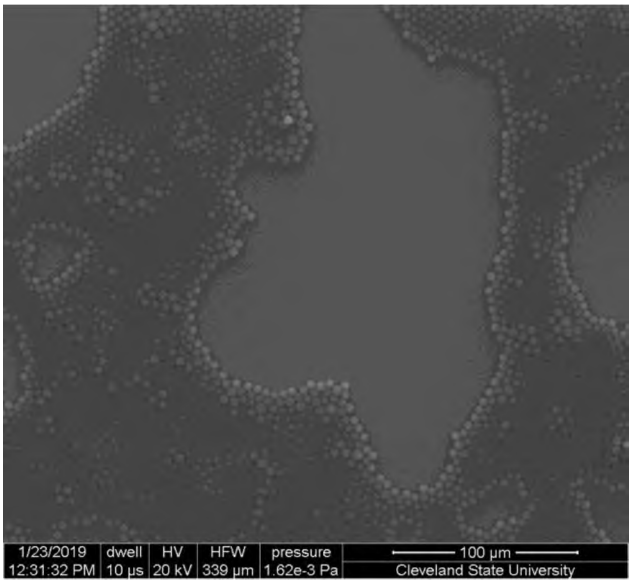

Figure 11: An SEM image of a covered wafer. Defects are identified by disorder in the packing of particles.

3.1.2 Platinum Deposition

Once the silicon wafers are coated with a monolayer of PS particles, the next step would be to deposit the metal on the top half of the particles. Depositing thin layers of metal can be done in a few ways. Some methods are dip coating, Langmuir-Blodgett, and physical/chemical vapor deposition. Physical vapor deposition (PVD) (DV-502A Turbo High Vacuum Evaporator) is the method that was available to us at a Case Western Reserve University facility (Materials for Opto/Electronics Research and Education Center) (**Figure 12**).

Figure 12: The Angstrom glovebox containing the components that make up the Physical Vapor Deposition (PVD) instrument. The platinum is placed in a crucible in the center and is evaporated upward onto the wafers.

The wafers are secured onto a tray with vacuum tape and screws, and inserted upside down, at the top of the PVD glovebox, above the crucible containing the platinum. Once the glovebox door is fastened shut, and it reaches a pressure <7.5x10-5 torr, an electron beam is targeted at the platinum, evaporating the metal at a rate of 1 A/s until a thickness of 20nm is reached [51].

3.2 Fluid cell assembly and experimental protocol

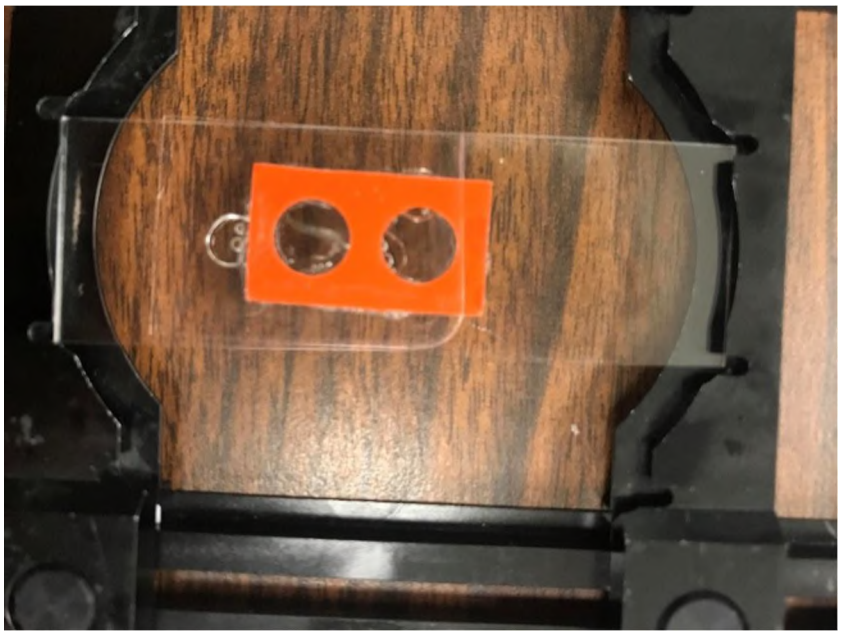

Figure 13: Particles suspended in peroxide. Spacers with 0.8 mm x 4.5 mm cells each with 7 μL of the particle suspension. The cells are screened for the best location to record (2-3% particle coverage and no bubbles). This example here shows intense bubbling and leaking of the fluid cell (18% H_2O_2 concentration).

After coating, the Janus particles were then introduced to hydrogen peroxide at defined peroxide and particle concentrations to be observed and studied. Peroxide concentration was changed systematically to test the effects of propulsion speed. The particle concentration was adjusted to result in videos that had particles cover 2-3% of the area of the recorded plane of view. Studies have suggested the range between 2%-10% as where living crystal clustering is observed. I chose to work on the lower limit of this range to avoid intense bubble formation with higher particle densities. **Figure 13** shows an example of a leaking fluid cell as a result of intense bubble formation. Similarly, I capped the particle density at 3% to avoid large differences in the number of particles in each video. Samples were vortex mixed upon mixing to further disturb the system and

thoroughly mix the particles. The sample was contained on the slide by adhesive spacers/isolators, then closed to the atmosphere with a microscope cover slide as shown in **Figure 14**.

Figure 14: A schematic of the fluid cell showing a side view of the spacers. The red disk represents the volume of the fluid cell within the adhesive spacer, not the adhesive spacer itself.

Each cell was observed under the microscope at 20x magnification, recording the first 30 minutes. As particles sediment, the particle density is not uniform across the entire fluid cell. Re-positioning the microscope over a portion of the bottom plane with a 2-3% coverage while also avoiding major bubble formation was a major difficulty and caused many videos to be discarded. Bubble formation becomes much more of a factor as hydrogen peroxide concentration increases (**Figure 15**). This caused the experiment range of peroxide concentration tested to be capped at 3%.

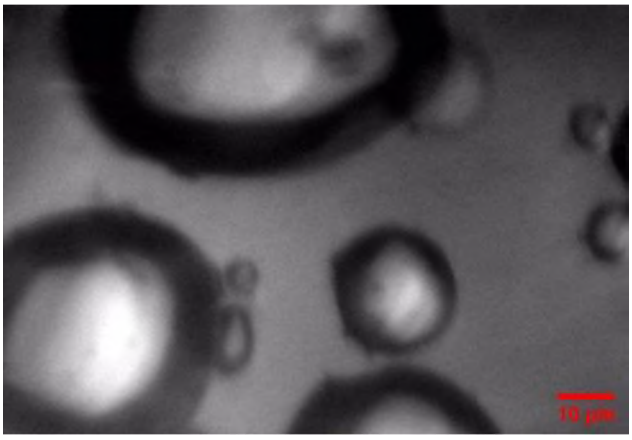

Figure 15: An image captured showing the bubble formation. H_2O_2 concentration was 18%. Bubble formation became a major issue as the rate of peroxide catalyzed by the platinum increased.

3.3 Image processing and data analysis

A camera (Hamamatsu ORCA-R2 C10600-10B) attached to a microscope (Olympus BX51WI) captured images of the sample at a rate between 8-16.2 frames per second (fps). The collection of images is then processed in ImageJ. First, the collection can be sliced to reduce size, keeping approximately an image at every 10 second interval of the video.

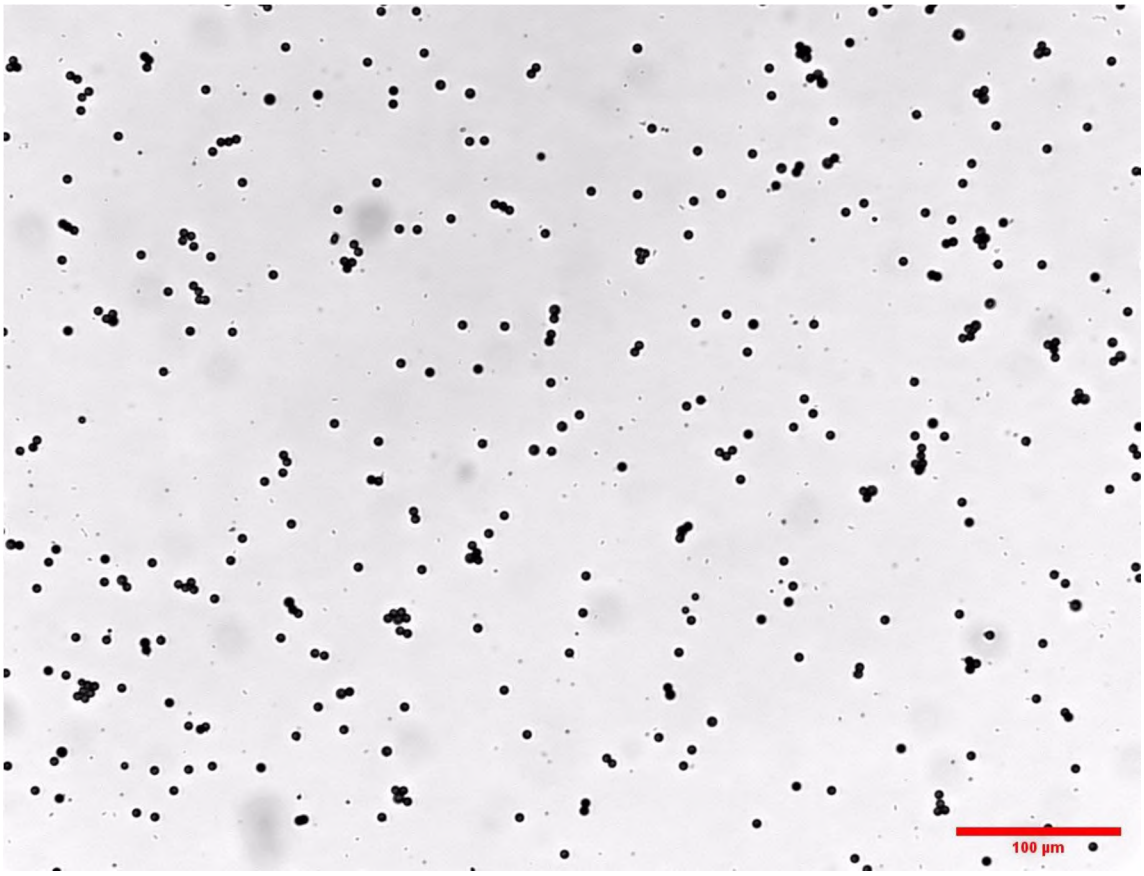

Figure 16: A standard image of Janus particles under the microscope. This is an unedited image directly after being recorded.

Microscope images showed the particles as dark while the background appeared light (**Figure 16**). Once the image is viewed in a greyscale, it can be further edited to show pixels as either completely white, or completely black, adding a strong contrast between

the particles and their background. This can be done by adjusting the pixel threshold of the images on ImageJ, showing darker pixels as 0s (black) and lighter pixels as 255s (white). This will leave holes inside some particles as light sometimes reflects off the center of particles making them appear lighter in color, but ImageJ offers an option to fill them. Once converted into binary images with full-bodied particles as shown in **Figure 17**, it can be further analyzed.

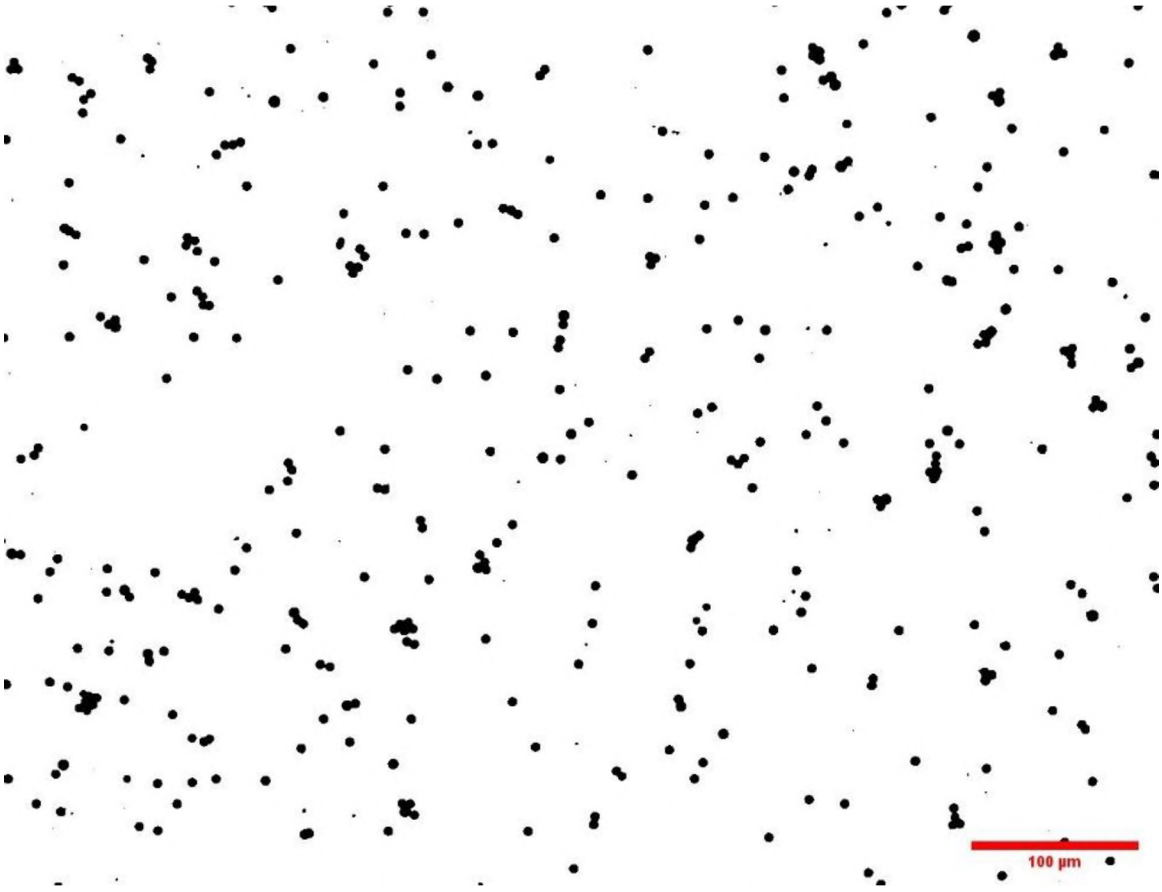

Figure 17: The same image from Figure 16 made binary. There is a greater contrast between the particles and the background. ImageJ also fills the light areas within particles caused by the reflection of the microscope light.

ImageJ offers the option to calculate the pixelated area of each object in every image. The area can be used to predict how many particles are in a certain object, given the average

observed area of a single particle. The diameter of the particles used is already known, and depending on the magnification used, an area can be calculated and converted into pixel units.

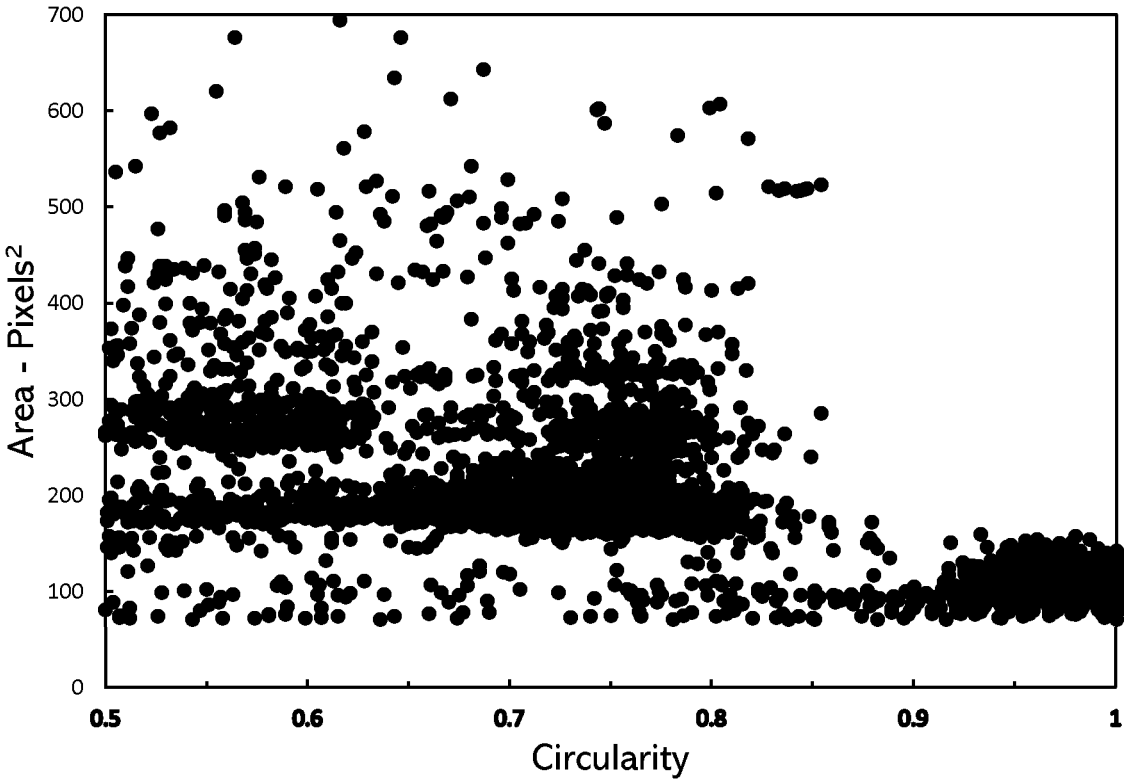

Figure 18: Area of objects under the microscope vs its circularity. There is a clear grouping of particles at circularity of 0.9 and above. Assuming only singlets will have high circularity, singlet particles can be systematically isolated from the rest of the observations.

Assuming 20x magnification (0.5119um/pixel), the average cross-sectional singlet area should be 71.96 pixels^2, but observing the data from ImageJ as it appears in **Figure 18**, singlets appear slightly bigger with a range of 80-120 pixels^2. Thus, singlets were isolated from clustered observations and analyzed for an average. This can be done by assuming that only singlets will have a circularity near 1, which is another measurement that can be

analyzed using ImageJ. A plot of every particle's area against its circularity confirms this assumption. It is clear from the figure above that only singlets are observed at a circularity above 0.9. For further accuracy, 0.95 is used, and an average singlet area is calculated from live data from each frame itself, thus accounting for changes in microscopy settings from one frame to another.

$$\text{Cluster Size} \approx \frac{\text{Observed Area}}{\text{Area of a Singlet}} \tag{1}$$

Once the cluster size is known, cluster population figures can be constructed to test the effects of the changing parameters on the frequency a certain cluster size is observed. Cluster sizes were binned into three different classifications, singlets (1 particle), intermediates (2-3 particles) and clusters (4+ particles) and plotted vs time as seen in **Figure 19** below. Populations were binned into three classes due to the stochastic nature of clusters merging and exchanging particles.

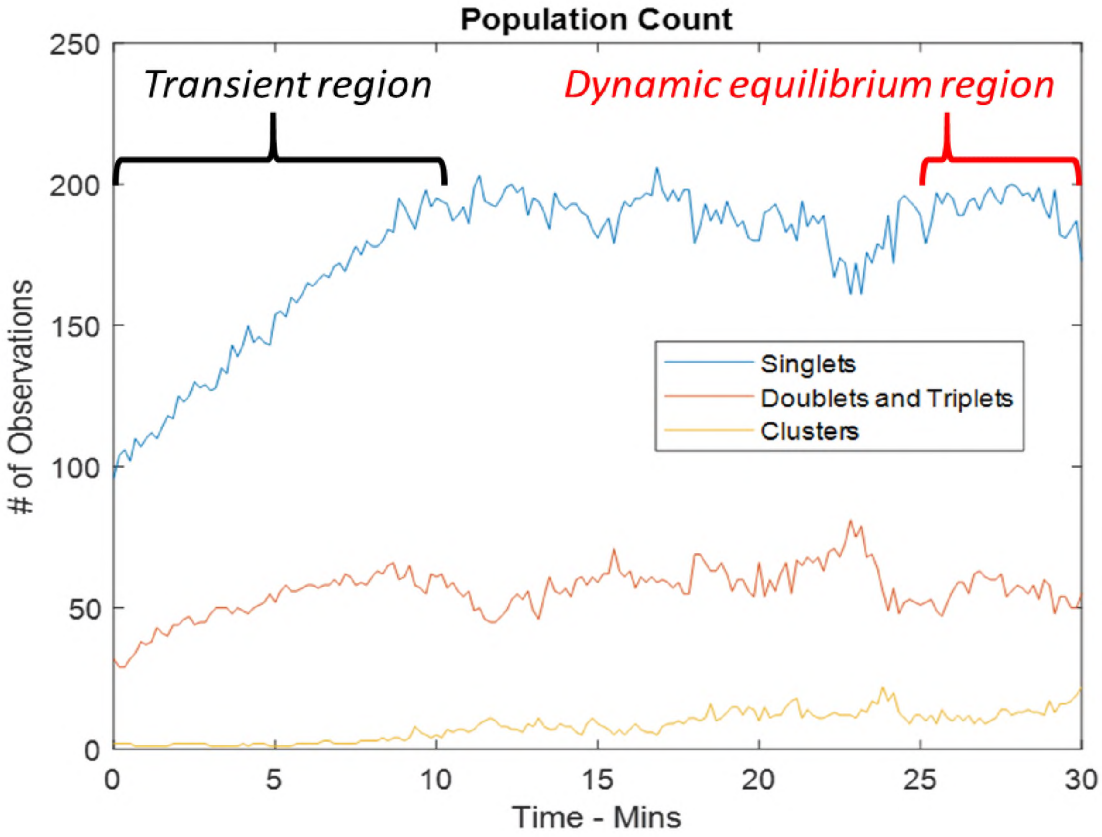

Figure 19: Plot of each population classification count vs time. The transient region was heavily influenced by sedimentation and the fluid cell settling. Once the effects of sedimentation wore off, the rate of clustering levels off into the dynamic equilibrium region.

Finally, total population counts were converted into probabilities by dividing each population count by the total number of observations in each frame. This is done to allow better comparison between different trials where the total number of observations varied, generally falling between 350-450. The equation is as follows:

$$\%\,\text{Observed} = \frac{N_i}{\sum_{i=1}^{3} N_i} \tag{2}$$

where N_i is the number of objects observed of that classification in a given frame and i indicates the classification of singlet (i = 1), intermediate (i = 2), and cluster (i = 3). Larger

values of percent observed for a given classification implies that a larger fraction of the total number of objects belong to that classification.

Furthermore, sedimentation had a very strong effect on the data throughout approximately the first ten minutes of each video (transient region). Once the effects of sedimentation wore off, each population count began leveling off into the dynamic equilibrium region where a mean of the number of observations was taken over the last five minutes and compared over the range of hydrogen peroxide concentrations tested.

CHAPTER IV

RESULTS AND DISCUSSION

Within the experiments described herein, I track cluster formation in real time using video microscopy to demonstrate the effect of swimming speed on collective behavior through varying fuel concentration. I varied hydrogen peroxide concentration from 0%-3% and used data to track the percentage of classified clusters observed over time within the region recorded by the microscope. Population counts showed enhanced clustering as fuel concentrations increased (**4.1**). I repeated experiments to verify results and once I was confident in the data that higher fuel concentrations led to enhanced cluster formation, I introduced a depletion interaction to the highest peroxide concentration tested (3%) to investigate its effects on clustering. Considering a previous study showing that depletion interactions quenched swimming speeds, it was expected that clustering would be reduced [23]. Thus, I varied the concentration of depletant added (PEG 6K) to the fuel concentration I observed most clustering at (3% hydrogen peroxide) to better demonstrate any quenching of clustering as a result, if at all. The experimental results did show a quenching of clustering in concentrations within the range where quenching of swimming speeds is

previously reported, however, lowering the depletant concentration showed enhanced clustering (**4.2**).

4.1 Effect of hydrogen peroxide on cluster formation

Based on previous work into this propulsion system, I expected cluster formation to increase with increased nominal speeds. Varying the speed here was done by increasing hydrogen peroxide concentration. Below, in **Figure 20**, I measure the evolution of singlets, intermediates, and clusters from a single trail of my experiments into 3% hydrogen peroxide as a function of time.

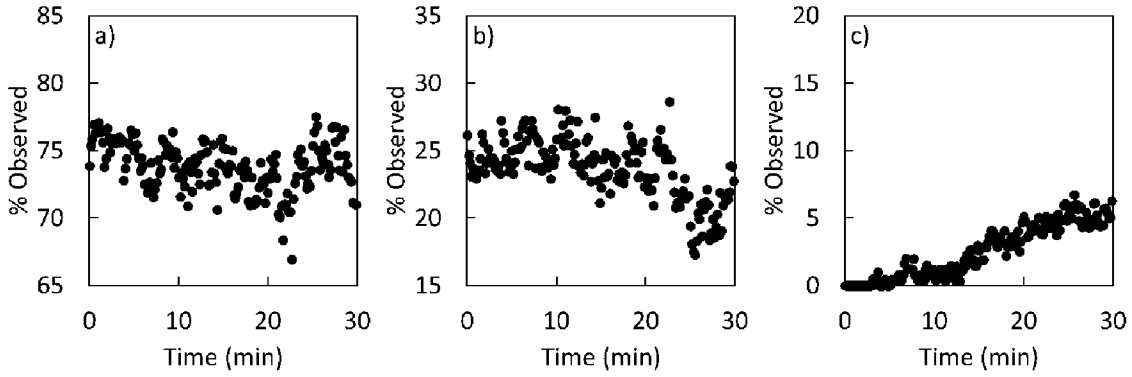

Figure 20: Evolution of a) singlets. b) intermediates. c) clusters. Measurements of singlets and intermediates had strong temporal fluctuations due to the dynamic merging and separating process of cluster formation and the influx of particles as a result of sedimentation early in the trial.

The probability of clusters observed increased from the beginning of the video at the expense of singlets and intermediates. However, the decrease in singlets was not as strongly as expected but is not surprising once I consider the effects of sedimentation over the early parts of recording. Furthermore, the singlet and intermediates showed much stronger temporal fluctuations than clusters due to the dynamic merging and breakdown of

aggregations in these populations. It is far more likely for a cluster observation of four particles or more to keep its "cluster" classification after losing or gaining another particle than it is for intermediates (singlets immediately change classification).

Next, the dynamic equilibrium mean for each classification was averaged over multiple trials of the same conditions and compared over increasing hydrogen peroxide concentration (**Figure 21**). Clustering dynamics of Janus particles were tracked for hydrogen peroxide concentrations between 0%-3%. Hydrogen peroxide was effectively used to increase the nominal speeds of particles, which in turn increased the probability of larger formations observed as evident by the increase of intermediates and clusters observed. On the other hand, I can see a clear decline in the probability of observing singlets as the hydrogen peroxide concentration which serves as a proxy for nominal speeds increased.

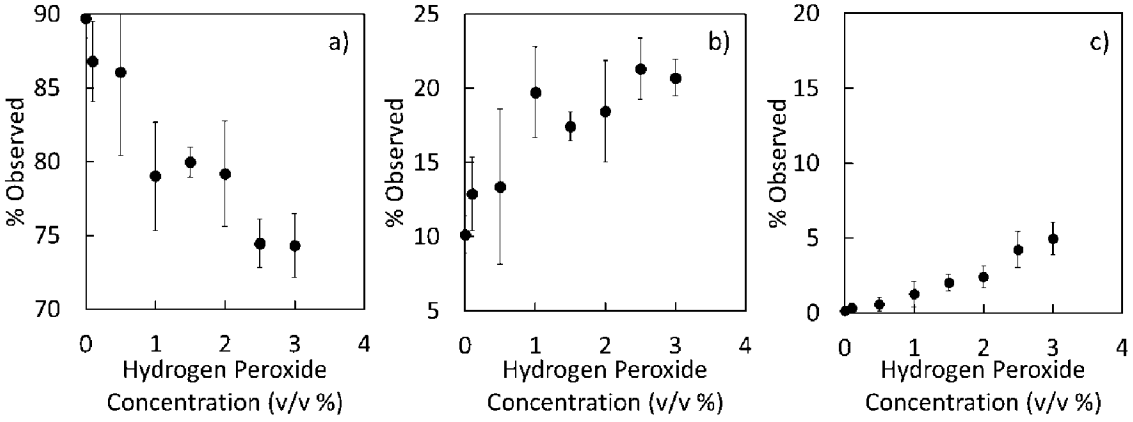

Figure 21: a) Singlet % Observed vs hydrogen peroxide concentration. b) Intermediate % Observed vs hydrogen peroxide concentration. c) Cluster % Observed vs hydrogen peroxide concentration. Cluster probabilities increased with increasing peroxide concentration, while singlets clearly declined. Intermediates experienced a sharp increase at first that leveled off at higher peroxide concentration as more clusters were formed.

Alternatively, I have averaged the cluster probability of every trial from each peroxide concentration tested and plotted them over time. The results from **Figure 22** not only confirm higher peroxide concentrations lead to higher cluster probabilities, but a case could be made for a faster rate of cluster formation.

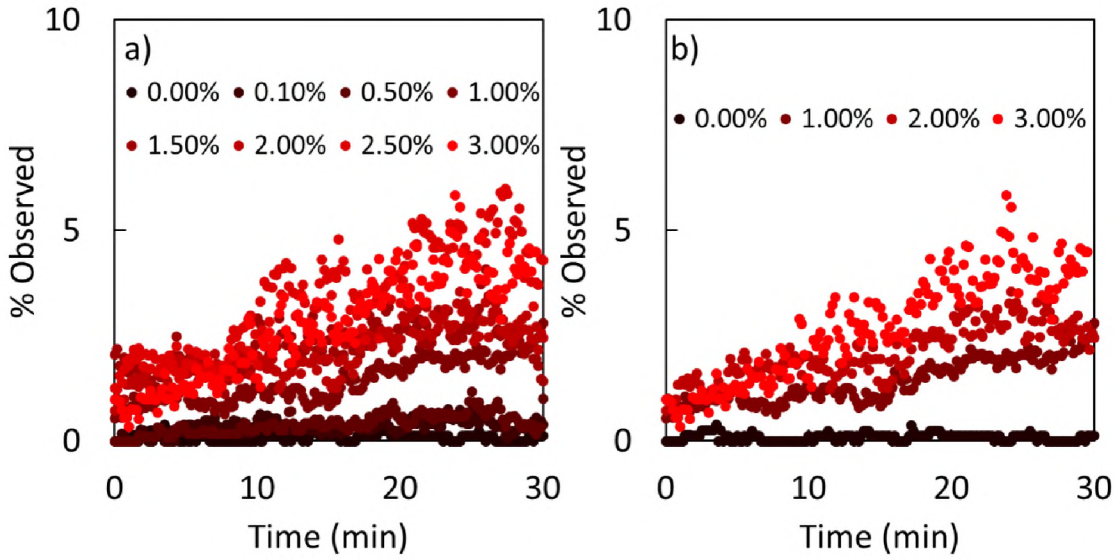

Figure 22: a & b) Evolution of clusters (4+) for active Janus particles in hydrogen peroxide. The intensity of red is proportional to the hydrogen peroxide concentration. Note that b displays the same data as a but with 4 data points removed for clarity.

4.2 Effects of depletants on cluster formation

Our lab's previous work has shown that the addition of depletants, specifically low molecular weight (6K) polyethylene glycol, reduced the propulsion speed of active Janus particles [23]. Here, I introduced systematically varied volume fractions of PEG (6K molecular weight) to a fixed hydrogen peroxide concentration of 3%. My experimental setup tested for volume fractions matching those of our lab's previous work where

propulsion speed was quenched, and lower. I believed that since clustering was a strong function of swimming speeds, that decreasing the apparent swimming speed would decrease the extent of clustering observed, even though I am keeping the rate of activity the same.

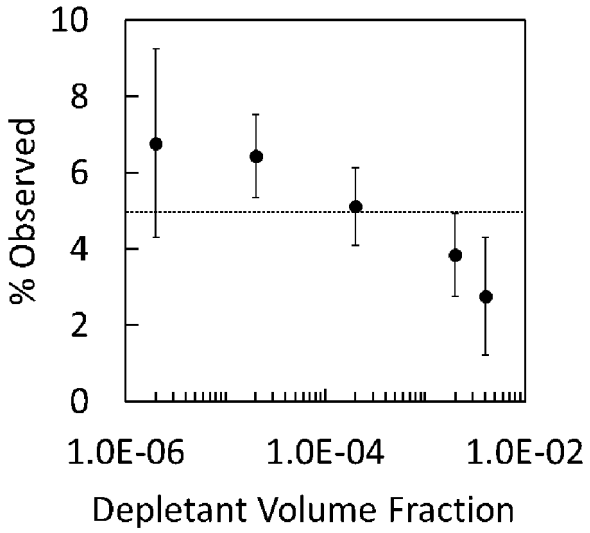

Figure 23: The extent of clustering at dynamic equilibrium for Janus particles in 3% hydrogen peroxide plotted over various volume fractions of PEG. The dotted line represents the % observed in the absence of PEG. The grey shaded area represents the region of volume fractions where propulsion speed was observed to be quenched. At low volume fractions, propulsion speed, and thus collision probability was likely unaffected, however the presence of depletants enhanced particle-to-particle attraction, in hand increasing cluster longevity. At high volume fractions, propulsion speeds are reduced, thus decreased the collision probability and extent of clustering.

Noting that the dashed line in **Figure 23** represents the probability of observing a cluster in 3% hydrogen peroxide without depletants, I can see that the addition of depletants initially enhanced clustering above that line but diminished as PEG volume fractions increased. More importantly to notice is that the probability of observing a cluster

decreased below the dashed line only once in the grey region. This grey region of the plot corresponds to the range of volume fractions where propulsion speeds were observed to be reduced by our lab's previous work. It is fair to assume that the addition of PEG quenched the propulsion speeds, thus reduced clustering as hypothesized by reducing the collision probability. On the other hand, the enhanced clustering at lower volume fractions is most likely due to increased particle-to-particle attraction due to the depletion interaction. At low depletant volume fractions, the apparent speed is roughly unchanged, meaning no significant changes to the collision probability. However, once particles collide and cluster, there is likely an enhanced attraction felt by particles introduced by the presence of depletants. It is important to note that particle to particle attraction would also further increase with increased volume fractions, however such attraction is on a sufficiently small length scales that the interaction becomes irrelevant for small collision probabilities. Finally, it is worth noting that at the highest PEG volume fraction tested, approximately 30% of the particles appear to be immobilized by bottom boundary as a result of the depletion interaction, significantly reducing the probability of collision.

CHAPTER V

CONCLUSION

Through this research, I have demonstrated a series of experiments investigating the effects of propulsion speed on the extent of clustering of active Janus particles in hydrogen peroxide. Clustering of 5 um catalytic active Janus particles was tracked with changes in hydrogen peroxide and depletant (PEG) concentration. Our results found that the extent of clustering increased by increasing the hydrogen peroxide concentration in the absence of PEG, which in turn, increases the apparent swimming speed and collision probability. This clustering was further enhanced by the addition of depletants at small volume fractions. However, after a certain point, the addition of more PEG will hinder clustering. The range of PEG volume fractions I found to hinder clustering corresponded to where I observed quenched swimming speeds. Based on this data, I conclude that increasing the collision probability of catalytic active Janus particles will increase cluster formation. Second, I conclude that the additions of PEG at low volume fractions enhances clustering by enhancing particle-to-particle attraction and increasing cluster longevity. On the other hand, high volume fractions reduce the collision probability, thus reduce clustering.

REFERENCES

[1] Paxton, W.; Kistler, K.; Olmeda, C.; Sen, A.; St. Angelo, S.; Cao, Y.; Mallouk, T.; Lammert, P.; Crespi, V. Catalytic Nanomotors: Autonomous Movement Of Striped Nanorods. Journal of the American Chemical Society 2004, 126 (41), 13424-13431.

[2] Deutsch, A.; Theraulaz, G.; Vicsek, T. Collective Motion In Biological Systems. Inerface Focus 2012, 2 (6), 689-692.

[3] Wadhams, G.; Armitage, J. Making Sense Of It All: Bacterial Chemotaxis. Nature Reviews Molecular Cell Biology 2004, 5 (12), 1024-1037.

[4] Ebbens, S. Active Colloids: Progress And Challenges Towards Realising Autonomous Applications. Current Opinion in Colloid & Interface Science 2016, 21, 14-23.

[5] Ebbens, S.; Howse, J. In Pursuit Of Propulsion At The Nanoscale. Soft Matter 2010, 6 (4), 726.

[6] Sengupta, S.; Ibele, M.; Sen, A. Fantastic Voyage: Designing Self-Powered Nanorobots. Angewandte Chemie International Edition 2012, 51 (34), 8434-8445.

[7] Yadav, V.; Duan, W.; Butler, P.; Sen, A. Anatomy Of Nanoscale Propulsion. Annual Review of Biophysics 2015, 44 (1), 77-100.

[8] Wang, J. Can Man-Made Nanomachines Compete With Nature Biomotors?. ACS Nano 2009, 3 (1), 4-9.

[9] Paxton, W.; Sundararajan, S.; Mallouk, T.; Sen, A. Chemical Locomotion. Angewandte Chemie International Edition 2006, 45 (33), 5420-5429.

[10] Shrivastava, A.; Patel, V.; Tang, Y.; Yost, S.; Dewhirst, F.; Berg, H. Cargo Transport Shapes The Spatial Organization Of A Microbial Community. Proceedings of the National Academy of Sciences 2018, 115 (34), 8633-8638.

[11] Das, S.; Garg, A.; Campbell, A.; Howse, J.; Sen, A.; Velegol, D.; Golestanian, R.; Ebbens, S. Boundaries Can Steer Active Janus Spheres. Nature Communications 2015, 6 (1).

[12] Uspal, W.; Popescu, M.; Dietrich, S.; Tasinkevych, M. Rheotaxis Of Spherical Active Particles Near A Planar Wall. Soft Matter 2015, 11 (33), 6613-6632.

[13] Buttinoni, I.; Bialké, J.; Kümmel, F.; Löwen, H.; Bechinger, C.; Speck, T. Dynamical Clustering And Phase Separation In Suspensions Of Self-Propelled Colloidal Particles. Physical Review Letters 2013, 110 (23).

[14] Theurkauff, I.; Cottin-Bizonne, C.; Palacci, J.; Ybert, C.; Bocquet, L. Dynamic Clustering In Active Colloidal Suspensions With Chemical Signaling. Physical Review Letters 2012, 108 (26).

[15] Bechinger, C.; Di Leonardo, R.; Löwen, H.; Reichhardt, C.; Volpe, G.; Volpe, G. Active Particles In Complex And Crowded Environments. Reviews of Modern Physics 2016, 88 (4).

[16] Duan, W.; Wang, W.; Das, S.; Yadav, V.; Mallouk, T.; Sen, A. Synthetic Nano- And Micromachines In Analytical Chemistry: Sensing, Migration, Capture, Delivery, And Separation. Annual Review of Analytical Chemistry 2015, 8 (1), 311-333.

[17] Campuzano, S.; Kagan, D.; Orozco, J.; Wang, J. Motion-Driven Sensing And Biosensing Using Electrochemically Propelled Nanomotors. The Analyst 2011, 136 (22), 4621.

[18] Wang, J. Cargo-Towing Synthetic Nanomachines: Towards Active Transport In Microchip Devices. Lab on a Chip 2012, 12 (11), 1944.

[19] Wang, J.; Gao, W. Nano/Microscale Motors: Biomedical Opportunities And Challenges. ACS Nano 2012, 6 (7), 5745-5751.

[20] Gao, W.; Wang, J. The Environmental Impact Of Micro/Nanomachines: A Review. ACS Nano 2014, 8 (4), 3170-3180.

[21] Würger, A. Self-Diffusiophoresis Of Janus Particles In Near-Critical Mixtures. Physical Review Letters 2015, 115 (18).

[22] Mozaffari, A.; Sharifi-Mood, N.; Koplik, J.; Maldarelli, C. Self-Diffusiophoretic Colloidal Propulsion Near A Solid Boundary. Physics of Fluids 2016, 28 (5), 053107.

[23] Issa, M.; Baumgartner, N.; Kalil, M.; Ryan, S.; Wirth, C. Charged Nanoparticles Quench The Propulsion Of Active Janus Colloids. ACS Omega 2019, 4 (8), 13034-13041.

[24] Moran, J.; Posner, J. Electrokinetic Locomotion Due To Reaction-Induced Charge Auto-Electrophoresis. Journal of Fluid Mechanics 2011, 680, 31-66.

[25] Wang, S.; Wu, N. Selecting The Swimming Mechanisms Of Colloidal Particles: Bubble Propulsion Versus Self-Diffusiophoresis. Langmuir 2014, 30 (12), 3477-3486.

[26] Gibbs, J.; Zhao, Y. Autonomously Motile Catalytic Nanomotors By Bubble Propulsion. Applied Physics Letters 2009, 94 (16), 163104.

[27] Mei, Y.; Solovev, A.; Sanchez, S.; Schmidt, O. Rolled-Up Nanotech On Polymers: From Basic Perception To Self-Propelled Catalytic Microengines. Chemical Society Reviews 2011, 40 (5), 2109.

[28] Magdanz, V.; Guix, M.; Schmidt, O. Tubular Micromotors: From Microjets To Spermbots. Robotics and Biomimetics 2014, 1 (1).

[29] Howse, J.; Jones, R.; Ryan, A.; Gough, T.; Vafabakhsh, R.; Golestanian, R. Self-Motile Colloidal Particles: From Directed Propulsion To Random Walk. Physical Review Letters 2007, 99 (4).

[30] Ebbens, S.; Gregory, D.; Dunderdale, G.; Howse, J.; Ibrahim, Y.; Liverpool, T.; Golestanian, R. Electrokinetic Effects In Catalytic Platinum-Insulator Janus Swimmers. EPL (Europhysics Letters) 2014, 106 (5), 58003.

[31] Chiang, T.; Velegol, D. Localized Electroosmosis (LEO) Induced By Spherical Colloidal Motors. Langmuir 2014, 30 (10), 2600-2607.

[32] Brown, A.; Poon, W. Ionic Effects In Self-Propelled Pt-Coated Janus Swimmers. Soft Matter 2014, 10 (22), 4016-4027.

[33] Nikolov, S.; Shum, H.; Balazs, A.; Alexeev, A. Computational Design Of Microscopic Swimmers And Capsules: From Directed Motion To Collective Behavior. Current Opinion in Colloid & Interface Science 2016, 21, 44-56.

[34] Wang, W.; Duan, W.; Ahmed, S.; Sen, A.; Mallouk, T. From One To Many: Dynamic Assembly And Collective Behavior Of Self-Propelled Colloidal Motors. Accounts of Chemical Research 2015, 48 (7), 1938-1946.

[35] Tailleur, J.; Cates, M. Statistical Mechanics Of Interacting Run-And-Tumble Bacteria. Physical Review Letters 2008, 100 (21).

[36] Palacci, J.; Sacanna, S.; Steinberg, A.; Pine, D.; Chaikin, P. Living Crystals Of Light-Activated Colloidal Surfers. Science 2013, 339 (6122), 936-940.

[37] Hieronimus, R.; Raschke, S.; Heuer, A. How To Model The Interaction Of Charged Janus Particles. The Journal of Chemical Physics 2016, 145 (6), 064303.

[38] Bayati, P.; Najafi, A. Dynamics Of Two Interacting Active Janus Particles. The Journal of Chemical Physics 2016, 144 (13), 134901.

[39] Ginot, F.; Theurkauff, I.; Detcheverry, F.; Ybert, C.; Cottin-Bizonne, C. Aggregation-Fragmentation And Individual Dynamics Of Active Clusters. Nature Communications 2018, 9 (1).

[40] Liebchen, B.; Löwen, H. Which Interactions Dominate In Active Colloids?. The Journal of Chemical Physics 2019, 150 (6), 061102.

[41] Leite, F.; Bueno, C.; Da Róz, A.; Ziemath, E.; Oliveira, O. Theoretical Models For Surface Forces And Adhesion And Their Measurement Using Atomic Force Microscopy. International Journal of Molecular Sciences 2012, 13 (12), 12773-12856.

[42] Spagnolie, S.; Lauga, E. Hydrodynamics Of Self-Propulsion Near A Boundary: Predictions And Accuracy Of Far-Field Approximations. Journal of Fluid Mechanics 2012, 700, 105-147.

[43] Shen, Z.; Würger, A.; Lintuvuori, J. Hydrodynamic Interaction Of A Self-Propelling Particle With A Wall. The European Physical Journal E 2018, 41 (3).

[44] Volpe, G.; Buttinoni, I.; Vogt, D.; Kümmerer, H.; Bechinger, C. Microswimmers In Patterned Environments. Soft Matter 2011, 7 (19), 8810.

[45] Uspal, W.; Popescu, M.; Dietrich, S.; Tasinkevych, M. Self-Propulsion Of A Catalytically Active Particle Near A Planar Wall: From Reflection To Sliding And Hovering. Soft Matter 2015, 11 (3), 434-438.

[46] Tuinier, R. Introduction To Depletion Interaction And Colloidal Phase Behaviour. Soft Matter at Aqueous Interfaces 2015, 71-106.

[47] Ziębacz, N.; Wieczorek, S.; Kalwarczyk, T.; Fiałkowski, M.; Hołyst, R. Crossover Regime For The Diffusion Of Nanoparticles In Polyethylene Glycol Solutions: Influence Of The Depletion Layer. Soft Matter 2011, 7 (16), 7181.

[48] Marenduzzo, D.; Finan, K.; Cook, P. The Depletion Attraction: An Underappreciated Force Driving Cellular Organization. Journal of Cell Biology 2006, 175 (5), 681-686.

[49] Lele, B.; Tilton, R. Control Of The Colloidal Depletion Force In Nonionic Polymer Solutions By Complexation With Anionic Surfactants. Journal of Colloid and Interface Science 2019, 553, 436-450.

[50] He, Y.; Zhu, B.; Zeng, X.; Yang, R.; Lv, X.; Yuan, W. Fabrication Of Large-Area, Close-Packed, Monolayer Colloidal Crystals Via A Hybrid Method Of Spin Coating And Peeling–Draining. Thin Solid Films 2017, 639, 98-106.

[51] Pawar, A.; Kretzschmar, I. Multifunctional Patchy Particles By Glancing Angle Deposition. Langmuir 2009, 25 (16), 9057-9063.

APPENDICES

A. Harvest Procedure

Sample Harvest Procedure:

- Submerge substrate (silicon wafer) in DI water (Approx. 12-15 mL in 50 mL centrifuge tube).
- Bath sonicate for 20 mins.
- Remove silicon wafer from suspension.
- Centrifuge for 20 mins at 1000 RPM.
- Remove supernatant (apporx 10 mL).
- Vortex mix remaining suspension volume (2-5 mL).
- Transfer suspension to 15 mL centrifuge tube.
- Centrifuge again for 20 mins at 1000 RPM.
- Remove supernatant, leaving behind 0.5-1 mL of suspension.
- Vortex mix suspension.
- Transfer suspension to microcentrifuge.
- Label and store.

B. Monolayer formation

Note: gloves are always to be worn while handling silicon wafers to avoid any contamination while tweezers are recommended to move wafers around.

Note: The proper concentration of polystyrene solution needed to make a monolayer varies based on temperature, humidity, particle size among other factors. Research, trial and error are recommended to find the best concentration as it changes based on the time of the year and the conditions then.

- Start with concentrations previously reported to work (Ex: 16% w/v for 5 μm and 8% w/v for 3 μm). Use recommendations of relatively sized particles if no previous information is available.
- In the case no previous information is available, the best trial and error method is to prepare the first solution with a high concentration (≈20%) and decrease the % by 0.5-1% each time with ethanol addition till the desired concentration is reached and recorded.

Solution Preparation:

- Use sonication bath and vortex mixer to properly disperse particles in the original storage bottle. Avoid using long bath sonication times. (~40 minutes)
- Note: Sulfated PS particles are stored in the refrigerator and must be placed back immediately after use.
- Transfer desired volume of solution into a small centrifuge tube. (1 mL tubes)

- Centrifuge at low speed (≈1000 RPM) till particles are completely separated from supernatant. First separation might take a longer time (≈>30 mins) compared to after particles are suspended in ethanol (≈5 mins).
- Take out the supernatant layer. Replace exact volume taken out with ethanol.
- Note: While removing supernatants, make sure the pipette tip does not come in contact with the lower region of the centrifuge tube to avoid withdrawing particles.
- It is best to set pipette to draw out a known volume each time right above the particles and replacing it with the same exact volume of ethanol to avoid changing the concentration too much. It is okay to leave small amounts of the supernatant layer as it will be removed over multiple washes.
- Use bath sonication and vortex mixing to disperse particles once again. Avoid long sonication times as particles are known to accumulate charge over time in the bath which could lead to clumps and impurities in the monolayer. (~30 mins)
- Once particles are completely dispersed and mixed in solution, repeat the separation and wash process 5-10 times.
- On the last separation/wash, adjust the amount of ethanol added to end at the goal particle concentration for the monolayer formation process.

C. Image Analysis MATLAB code

```
clear,clc


%Particle Data Entry
filename = 'Results.CSV'; %Edited Individual Particle Data
PN= xlsread('Results.CSV','A:A'); %Particle Number/First Column%
PA= xlsread('Results.CSV','B:B'); %Particle Area/Second Column%
S= xlsread('Results.CSV','E:E'); %Slice Location/Fifth Column%
C= xlsread('Results.CSV','C:C'); %Circlarity/Third Column%

%Slice Data Entry
filename = 'Summary.CSV'; %Edited Slice Data
PC= xlsread('Summary.CSV','B:B'); %Particle Count/Second Column%
TA= xlsread('Summary.CSV','C:C'); %Total Area/Third Column%
ACA= xlsread('Summary.CSV','D:D'); %Average Cluster Area/Fourth Column%
AF= xlsread('Summary.CSV','E:E'); %Area Fraction/Fifth Column%

%Singlet Average Area Loop%
NS=1; %Singlet particle Counter
NR=1; %Determine The Range of Particles To Analyze Area For
NPC=1; %Counter for Range of Particles Lower Limit Counter
NPCF=PC(1); %Range of Particles Upper Limit
for U=1:S(end)
   for N=NR:NPCF
      if C(N)>=0.95 %Circlarity Threshold for Singlets
         SA(NS)=PA(N); %Singlet Area Indexed
         NS=NS+1; %Singlet counter
      end
   end
   SAA(U)=mean(SA);
   SA=[];
   NS=1;
   if NPC<length(PC);
   NR=NR+PC(NPC);
   NPCF=NPCF+PC(NPC+1);
   NPC=NPC+1;
   end
end




%Population Count loop
```

```
TPC=zeros(S(end),1);
Z=zeros(S(end),5);%Population Matrix/5 types of clusters(1, 2, 3, 4, 5+)
for M=1:S(end)
   T(M) = (10/60) * (M - 1); %Time/Change Time Step%
   for N=1:length(PN)
      CS(N)=round(PA(N)/SAA(M));
      if S(N)==M
         TPC(M)=TPC(M) + CS(N);
         if CS(N)==1
            Z(M,1)=Z(M,1)+1;
         elseif CS(N)==2
            Z(M,2)=Z(M,2)+1;
            elseif CS(N)==3
            Z(M,3)=Z(M,3)+1;
               elseif CS(N)==4
            Z(M,4)=Z(M,4)+1;
                  elseif CS(N)>4
            Z(M,5)=Z(M,5)+1;

         end
      end
   end
end

% Finalizing Population Counts

ZZ(:,1)=Z(:,1);
ZZ(:,2)=Z(:,2)+Z(:,3);
ZZ(:,3)=Z(:,4)+Z(:,5);
NPC=(ZZ(:,1)+ZZ(:,2)+ZZ(:,3));


%Probability

P=(ZZ./NPC)*100;

%Plotting/Data Presentation


%Figure 1: Summary
figure('name','Summary')
subplot(2,1,1)
yyaxis left
plot(T,PC)
xlabel('Time - Mins')
ylabel('# of Clusters')
```

```
hold on
yyaxis right
plot(T,AF)
ylabel('%')
hold off
title('Cluster Count vs Area Fraction of the Particles')
legend('Cluster Count','Area Fraction of Particles')
legend('Location','northwest')
subplot(2,1,2)
plot(T,ACA)
xlabel('Time - Mins')
ylabel('Pixels^2')
title('Average Cluster Area')


%Figure 2: Population
figure('name','Population Count')
plot(T,ZZ(:,1),T,ZZ(:,2),T,ZZ(:,3))
title('Population Count')
ylabel('# of Observations')
xlabel('Time - Mins')
legend('Singlets','Doublets and Triplets','Clusters')
legend('Location','best')

% %Figure 3:Population Bar Chart
% figure('name','Population: Bar Chart')
% bar(ZZ)
% title('Population Count')
% ylabel('# of Observations')
% xlabel('Time - Mins')
% legend('Singlets','Doublets and Triplets','Clusters')

%Figure 3: Probability Chart
figure('name','Probability Count')
plot(T,P(:,1),T,P(:,2),T,P(:,3))
title('Probability')
ylabel('%')
xlabel('Time - Mins')
legend('Singlets','Doublets and Triplets','Clusters')
legend('Location','best')

% %Figure 5:Probability Bar Chart
% figure('name','Probability: Bar Chart')
% bar(P)
% title('Probability Count')
% ylabel('%')
```

```
% xlabel('Time - Mins')
% legend('Singlets','Doublets and Triplets','Clusters')

%Figure 4: Population Individual
figure('name','Population Count: Isolated')

subplot(3,2,[1,2])
plot(T,ZZ(:,1))
title('Singlet')
ylabel('# of Observations')
xlabel('Time - Mins')

subplot(3,2,[3,4])
plot(T,ZZ(:,2))
title('Doublets and Triplets')
ylabel('# of Observations')
xlabel('Time - Mins')

subplot(3,2,[5,6])
plot(T,ZZ(:,3))
title('Clusters')
ylabel('# of Observations')
xlabel('Time - Mins')


%Figure 5: Probability Individual
figure('name','Probability: Isolated')

subplot(3,2,[1,2])
plot(T,P(:,1))
title('Singlet')
ylabel('% of Observations')
xlabel('Time - Mins')

subplot(3,2,[3,4])
plot(T,P(:,2))
title('Doublets and Triplets')
ylabel('% of Observations')
xlabel('Time - Mins')

subplot(3,2,[5,6])
plot(T,P(:,3))
title('Clusters')
ylabel('% of Observations')
xlabel('Time - Mins')
```

```
%Figure 6: Total Particles
figure('name','Total Overall Particles vs Time')
plot(T,TPC)
title('Total Individual Particle Count')
ylabel('# of Individual Particles')
xlabel('Time - Mins')
```